Techno-Science Research Journal V13 (3) (2025) P 44-51

I.T.C

Content list available at ITC

Techno-Science Research Journal

Journal Homepage: http://techno-srj.itc.edu.kh/

Techno-Science Research Journal

Land Use and Land Cover Distribution across Litho-Mineral Alteration of an Irrigated Catchment of the Tonle Sap Lake, Cambodia

Kakda Pov[1], Chhenglang Heng[1,2], Makara Soy[1], Vincent Herbreteau[1,2], Vannak Ann[1,2*]

[1] *Research and Innovation Center, Institute of Technology of Cambodia, Russian Federation Blvd., P.O. Box 86, Phnom Penh, Cambodia*

[2]*Espace-Dev, IRD, Univ Montpellier, Univ Guyane, Univ La Réunion, Univ Antilles, Univ Nouvelle Calédonie, Montpellier, France*

Received: 31 August 2024; Revised: 18 November 2024; Accepted: 13 December 2024; Available online: December 2025

Abstract: *Characterized by a predominantly agricultural landscape, including rice paddy, agricultural land, and scattered forest, the Chrey Bak catchment of the Tonle Sap Lake, Cambodia, is experiencing challenges such as deforestation and land conversion, which negatively impact mineral alteration sources, land management, and ecosystems. The current study uses satellite data (Sentinel 2, Landsat-8 OLI, and ASTER) to detect changes in mineral alteration (i.e., iron oxide and clay) and in land use and land cover (LULC) and to examine their relationships with the catchment's lithology. Sentinel-2 satellite imagery between 2015 and 2022 was used to classify LULC changes. The visible and near-infrared (VNIR) and the short-wave infrared (SWIR) bands were used to map the iron oxide and clay deposits, thereby reducing the time and cost associated with fieldwork. The results revealed significant LULC changes, with a decrease in vegetated areas and an increase in cropland and built-up areas, while remaining unchanged for forested areas and water bodies. These changes have direct implications for mineral alteration, as the areas with land conversion (i.e., agricultural areas) showed their exposure to mineral-rich areas, particularly those containing iron oxide and clay. This study contributes to a qualitative understanding of the relationships between LULC changes across litho-mineral substrates, offering insights that can inform sustainable land management practices and mineral exploration efforts in the catchment.*

Keywords: Satellite images, time series, minerals, land cover dynamics

1. INTRODUCTION

Land use and land cover (LULC) changes are the study of land cover dynamics on the Earth's surface by land use (such as vegetation, cropland, and built-up area), describing human activity, while land cover is to study what covering the surface of the Earth, such as forests, wetlands, bare soils, and so on. This is achieved through Earth observation satellites, which study LULC changes at different dates to monitor their dynamics [1]. Human activities and natural processes can significantly affect minerals' physical and chemical properties, impacting ecosystem health, rock characteristics, soil fertility, and land management. LULC, including forested areas, agricultural lands, and water bodies, plays a crucial role in regulating the presence of litho-minerals, particularly iron oxide and clay, in irrigated catchments [2]. In recent years, rapid LULC changes have raised concerns about the long-term sustainability of those irrigated catchments. As agricultural lands and urban areas expand, forests and natural areas are cleared. This leads to an increasing disturbance of the iron oxide and clay's distribution and their depletion, these minerals being vital for maintaining soil structure [3]. If LULC changes too quickly, it can impact the health of the ecosystems [4]. To address this issue, Geographic Information Systems (GIS) and remote sensing techniques offer a powerful and efficient way to monitor spatiotemporal changes in LULC. These techniques allow us to observe large areas and investigate correlations between LULC changes and the underlying disturbance of the two minerals [5]. Integrating data from multispectral sensors, such as those onboard Lansat-8 OLI, ASTER, and Sentinel-2 satellites, can help detect mineral alteration and the relationships between LULC changes and the distribution of iron oxide and clay [6].Furthermore, it can also help to identify potential mining resource sites [6]. This study aims to link qualitatively the distribution of iron oxide and clay with the LULC changes in the Chrey Bak catchment of the Tonle Sap Lake (TSL), Cambodia.

* Corresponding author: Vannak Ann
E-mail: ann.v@itc.edu.kh*; Tel: +855-12 563 170*

2. METHODOLOGY

2.1 Study area

The geology of Mainland Southeast Asia comprises stratigraphic and intrusive igneous units, highlighting its richness in mineral resources [7]. Cambodia, located in Indochina's southernmost craton, hosts significant mineralization belts like the Truong Son Fold Belt (TSFB), Loei Fold Belt (LFB), Dalat-Kratie Belt (DKB), and Sukhothai Belt. Granitic magmatism, driven by the Indosinian orogeny, is linked to Gondwanaland fragment collisions (Fig. 1).

The Chrey Bak catchment is approximately 89 kilometers west of Phnom Penh, the capital city of Cambodia. This catchment is located at the Stueng Boribo, one of the tributaries of the TSL watershed.

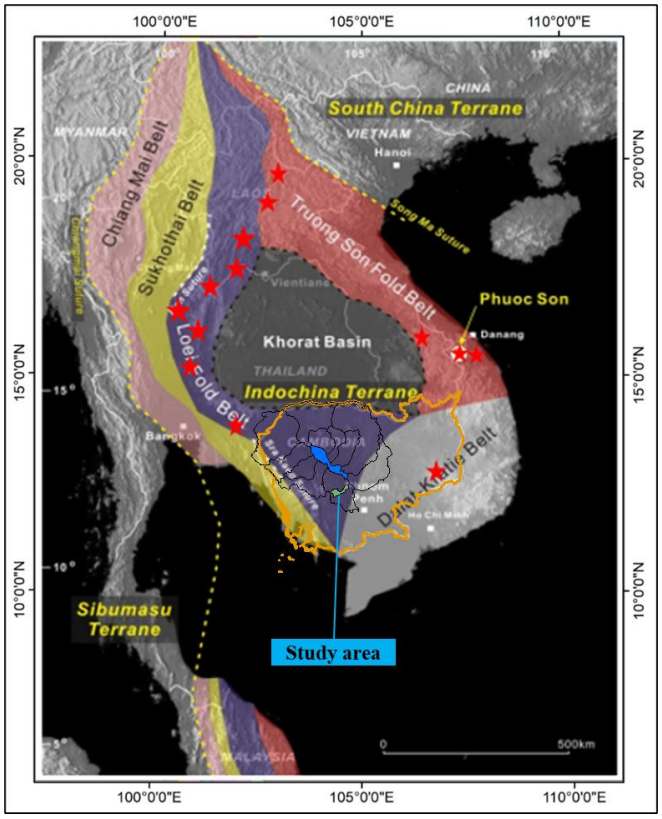

Fig. 1. Map showing tectonic divisions of the Indochina Terrane including the mineralization belt of Cambodia Vietnam, Laos, and Thailand (modified after [7]).

The lithology of the catchment is characterized by various rock types (JICA, 2002) that significantly influence its mineral potential. The iron oxide and clay are rich in deposits near dacites, granites, and hornfels, then erosion, transportation by weathering (raining, wind), and deposited in the eluvial sand, old alluvium, and recent alluvium (Fig. 2).

2.2. Image analysis

2.2.1 Image pre-processing

The Landsat-8 OLI and Terra ASTER images were pre-processed with ArcGIS 10.8 software in Universal Transverse Mercator (UTM) and projected to the World Geodetic System

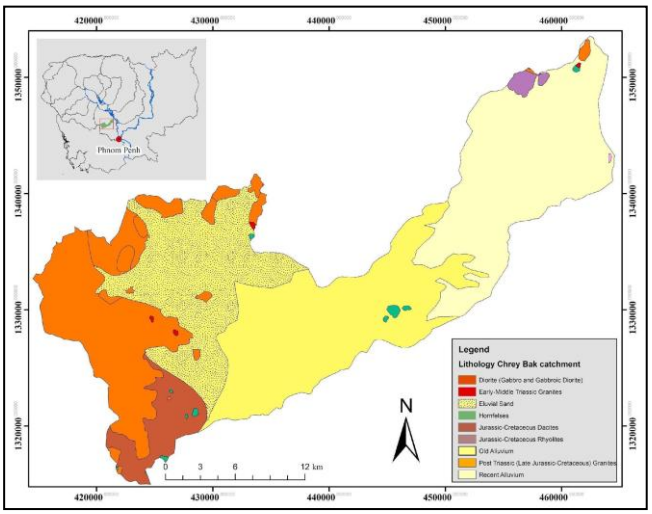

Fig. 2. Geological map of the Chrey Bak catchment, Kampong Chhnang province in Cambodia.

(WGS) 84 datum Zone 48N. They were converted to the Top-of-Atmosphere (TOA) spectral radiance [8], with radiometric calibration and atmospheric correction (following this formula: REFLECTANT_MULT_BAND × Band) + (REFLECTANT_ADD_BAND) / Sin(SUN_ELEVATION). The first step in this method was to enhance the spectral wavelength response of each iron oxide and clay in ArcGIS (Fig. 3). The classification of Sentinel-2 images in the present study included three steps: pre-processing of the images, training sampling manager, and support vector machine (SVM) algorithm to obtain final LULC classes. After completing the image preprocessing step, training sampling managers were chosen to encompass various potential LULC classes. Then, 80 pixels of training samples for each homogeneous class [9] were created to supervise the SVM classification process.

2.2.2 Sentinel-2 for LULC mapping

Sentinel-2 is equipped with the Multispectral Instrument (MSI), which captures data across 12 spectral bands ranging from the visible to the short-wave infrared spectrum, with spatial resolutions of up to 10 meters[10]. Sentinel-2 images from 2015 until 2022 in the catchment were classified using a support vector machine (SVM) algorithm. Typically, at least 80 samples per class are recommended to provide a reliable basis for classification [11]. The SVM algorithm is advantageous for handling high-dimensional data and distinguishing between classes with clear separations [11]. The analysis utilized the high-resolution imagery from Sentinel-2 to classify the LULC changes into several key categories: forest, vegetation, cropland, waterbody, built-up area, and LULC change (Fig. 6) In this study, specific bands such as bands 2, 3, 4, and 8 are used due to their

relevance in monitoring land use and land cover (LULC) changes. The primary objectives of Sentinel-2 imagery include monitoring agricultural lands, forests, and LULC classification [11]. Since Sentinel 2 data is multispectral, highly effective for accurately classifying LULC classes [12]. To assess the accuracy of the LULC classification, reference data, and high-resolution Google Earth imagery were used to create a confusion matrix compared with the classified data. This allowed us to calculate key accuracy metrics: the overall accuracy, the producer's accuracy, the user's accuracy, and the Kappa coefficient. Visualize the results to identify misclassification patterns and evaluate performance. If necessary, refine the classification by adjusting algorithm parameters or updating training data, and consider testing model robustness across different data sets [12].

2.2.3 Band ratio and principal component analysis

Band ratio has been one of the most widely used image enhancement methods to extract spectral information on any rocks and minerals using diagnostic absorption features at specific wavelength intervals. Landsat-8 OLI was launched in 2013 and its images include nine spectral bands, with bands 1 through 7, 8, and 9 having a spatial resolution of 30 meters [13]. In this study, specific bands such as bands 2, 4, 6, and 7 were used to observe spectral absorption characteristics across the visible and near-infrared (VNIR), shortwave infrared (SWIR), and thermal infrared (TIR) wavelength ranges, for detect only in 2015. These selected bands enhance the detection and analysis of geological and mineralogical features. Since the debut of Landsat-1 in 1972, satellite remote-sensing imagery has been extensively and successfully employed in mineral prospecting [13]. Landsat-8 OLI band ratio is used to calculate minerals: Iron oxide, with a band ratio of (b_4/b_2), is associated with mafic minerals like limonite, jarosite, hematite, and goethite; clay, with a (b_6/b_7), such as illite, kaolinite, alunite, and montmorillonite.

The Advanced Spaceborne Thermal Emission and Reflection Radiometer (ASTER) is particularly valuable, as it captures emitted and reflected electromagnetic radiation across 14 spectral bands: visible-near infrared (VNIR), shortwave infrared (SWIR), and thermal infrared (TIR). In this study, only specific ASTER bands (bands 1, 2, 5, 6, and 7) in 2015 are utilized due to their sensitivity to the spectral characteristic of minerals. ASTER's ability to provide comprehensive data on surface temperature, emissivity, reflectance, and elevation, combined with its reasonable spatial resolution, makes it an excellent tool for identifying minerals essential for mineral exploration. The band ratio for the mineral ASTER band in iron oxide with a band ratio of (b_2/b_1) absorption is 0.55 and 0.90 µm, with a peak near 0.75 µm, indicating a ferric iron abundance [14] S. Clay, with a $(b_5 \times b_7)/(b_6)^2$. Principal Components Analysis (PCA) image processing algorithms were used to obtain important information on minerals from the processed remote sensing datasets [14]. Most rational thematic layers of the modification are presented in order (Fig. 3). The Iron oxide from the Landsat-8 OLI image intersects with iron oxide from ASTER. The clay mineral from Landsat-8 OLI intersects with the clay mineral from ASTER.

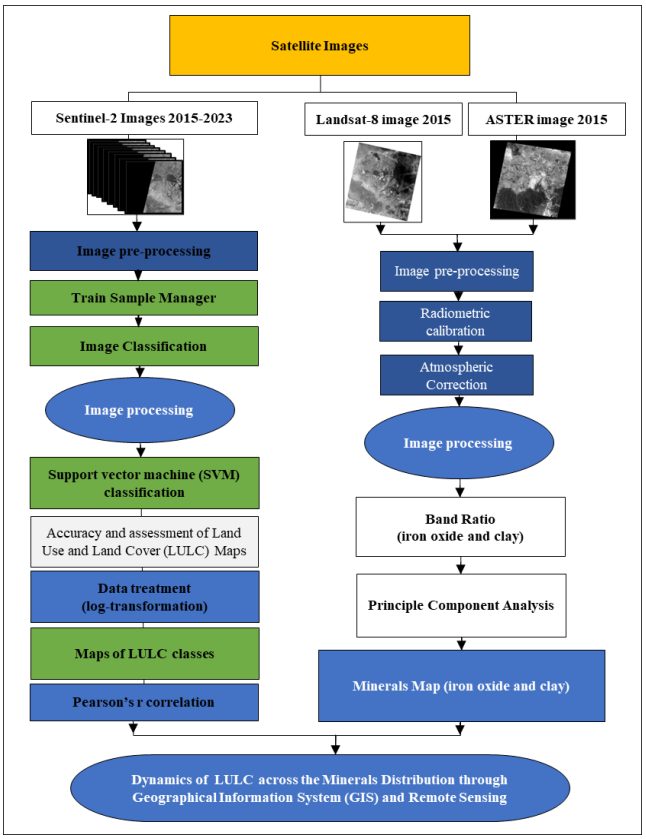

Fig. 3. The methodological flowchart to study land use and land cover (LULC) changes and mineral deposits in the Chrey Bak catchment.

2.3 Statistical analysis

The LULC classes in the irrigated catchment from 2015 to 2022 were log-transformed before conducting statistical analysis with R statistical software. The Pearson coefficient results, with *p-value* < 0.05 level, were considered significantly different.

3. RESULTS AND DISCUSSION

3.1 Spatial distribution of LULC across the litho-minerals

The lithological analysis identified six rock types: recent alluvium (27.20%), old alluvium (26.55%), granites (20.10%), eluvial sand (19.87%), diorite (5.14%), and dacites (0.66%) (Fig. 4). Based on the catchment's lithology, the old and recent alluviums are rich in iron oxide, while the granite and eluvial sand contain clay (Fig. 4). After detecting minerals on the six rocks of the catchment by using Landsat-8 OLI and Terra ASTER images, the result shows the percentage of minerals' distribution with the iron oxide (red color) being 22.63 % and clay (blue color) being 12.21 %. The old and recent alluviums are rich in iron oxide, and are significant for soil quality,

particularly in agricultural activities. Additionally, the granites and eluvial sand contain clay, which enhances soil fertility, water retention, and vegetation growth (Fig. 4 &Fig. 5).

The study period from 2015 to 2022 reveals the distribution of the LULC classes (forest, vegetation, cropland, water body, and built-up area). They were observed with the underlying

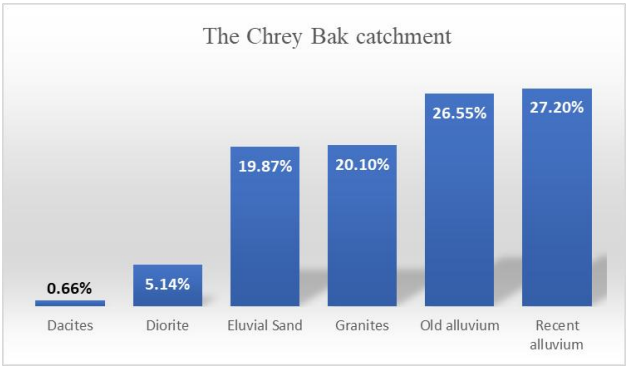

Fig. 4. The proportion of rock types in the Chrey Bak catchment.

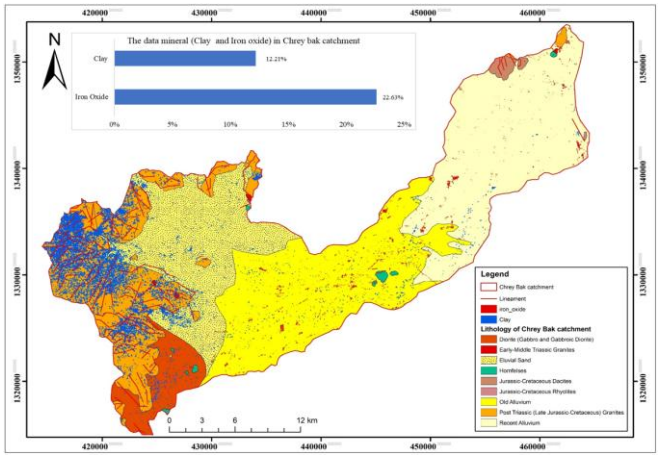

Fig. 5. The data percentage of minerals (iron oxide and clay) in the Chrey Bak catchment.

litho-minerals, such as dacite, diorite, eluvial sand, granite, old alluvium, and recent alluvium (Fig. 6). This analysis explores the interactions between the LULC classes and the minerals' distribution (iron oxide and clay), which are the key factors in determining LULC changes in the catchment. Clay-rich soils typically support specific forests and vegetation, while cropland types may not rely on clay minerals [15]. Iron minerals, crucial for certain croplands, may not be as critical for vegetation [16]. Cropland ranges from 47.14% to 64.07%, with an average of 57.32% and a standard deviation of 6.43%. This growth corresponds with the extensive presence of iron oxide in the old and recent alluviums, which increases agricultural productivity in the catchment over the years. The vegetation ranges between 19.07% and 37.50%, averaging 25.61% with a standard deviation of 7.22%; This primarily affects areas underlain by clay-rich granites and eluvial sand as the result of agriculture activities [17]. Similarly, the forest shows a more stable trend, ranging from 9.60% to 17.09% and averaging 13.38% with a standard deviation of 2.23%, primarily located in regions with clay minerals, which are increasingly threatened by agricultural expansion and urban development [18]. The built-up area ranges from 1.67% to 4.31% with an average of 2.94% and a standard deviation of 0.88%, reflecting urbanization and infrastructure growth [19]. Lastly, water bodies display high variability, ranging from 0.25% to 1.94%, averaging 0.75% with a standard deviation of 0.58%, reflecting the impacts of seasonal change and human interventions in water management (Fig. 6) [20].

The lithology in dacite shows vegetation predominance, with gradual increases in cropland and built-up areas. Forest cover is minimal due to less fertile soil conditions for agriculture [21]. In diorite, cropland is dominant, with a notable increase in built-up areas, particularly near infrastructure [21]. In eluvial sand, cropland remains dominant, with a slight reduction in forest cover and minimal growth in built-up areas. High iron oxide content drives agricultural expansion, especially in rice paddies [22]. In granites, forests and vegetation are more abundant, while cropland is secondary. The rich clay content supports forest growth, limiting agricultural and urban expansion [21]. In old alluvium, cropland consistently dominates, with slight increases in built-up areas. Iron oxide presence supports agricultural development, particularly for rice fields [22]. In recent alluvium, Cropland is the primary land use, with minimal growth in built-up areas. Rich in iron oxide, it supports extensive agricultural development, with minimal forest areas and moderate vegetation cover [22].

3.2 Time Series of LULC dynamics and their relationships

The LULC dynamics from 2015 to 2022 reveal significant changes in catchment due to deforestation, agriculture, and urbanization (Fig. 6&Fig. 7). Cropland increases, due to deforestation and land conversion for agriculture as shown in other studies, are the major factors. According to the FAO, agricultural expansion accounts for nearly 90% of global deforestation [16]. In (Table 1), forest cover shows correlations with agriculture, particularly cropland ($r = -0.86$, $p < 0.0001$), indicating that increasing agricultural activity might be related to deforestation. This result coincides with studies indicating that agricultural expansion is a major driver of deforestation [35], [37]. Forest and water bodies correlate ($r = -0.67$, $p < 0.01$), suggesting a spatial separation due to land use pressures near water resources impacted because ponds or ravines were filled by sheet erosion [32]. Forest and built-up areas also show a significant correlation ($r = -0.95$, $p < 0.0001$), highlighting the negative impact of urbanization on forests, as a forest is often the first to be cleared for residential, commercial, or industrial development [45]. Vegetation decreases are often due to land conversion for agriculture or urbanization and agricultural land conversion is a major driver of forest loss [23].

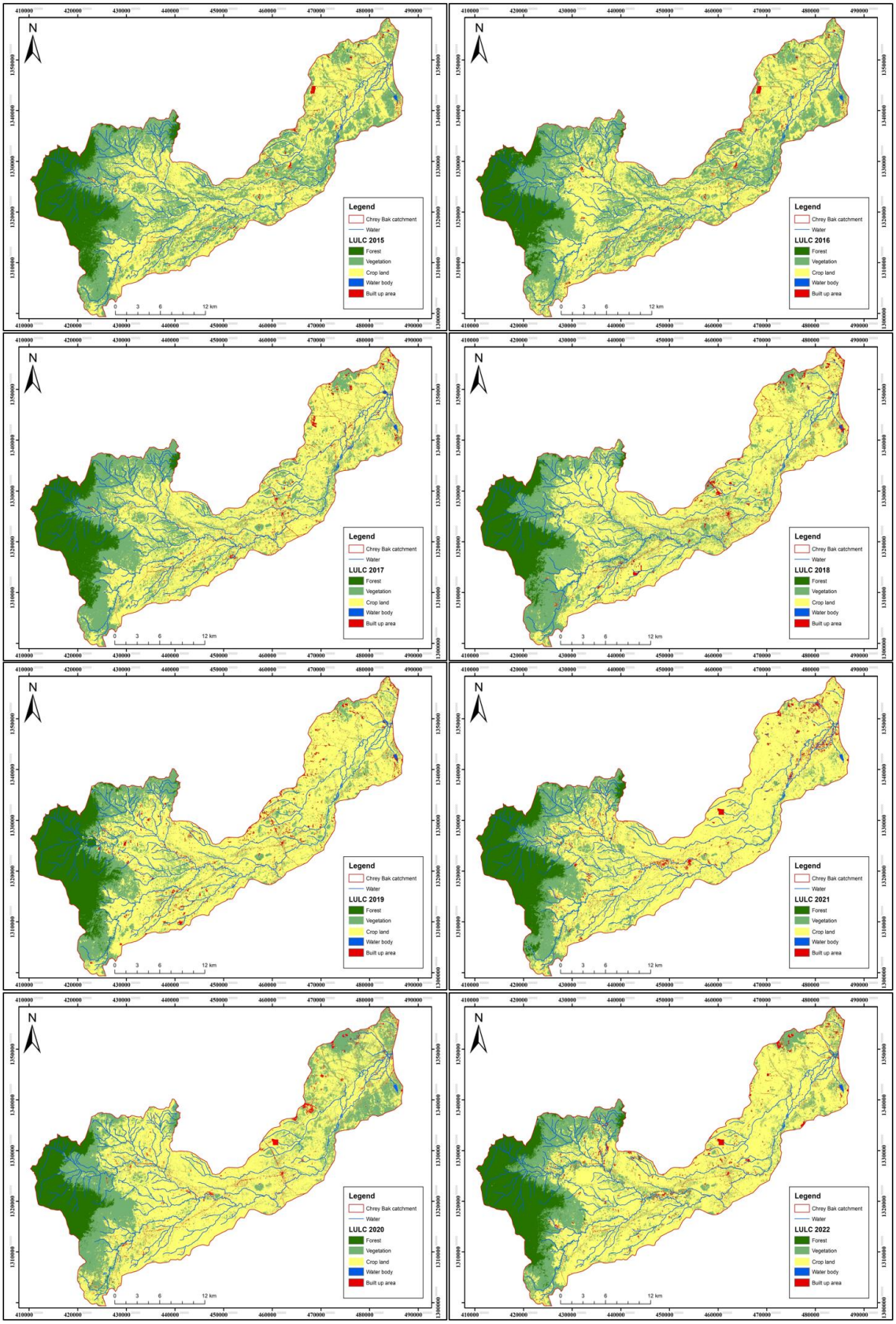

Fig. 6. Maps of LULC distribution in the Chrey Bak catchment from 2015 to 2022.

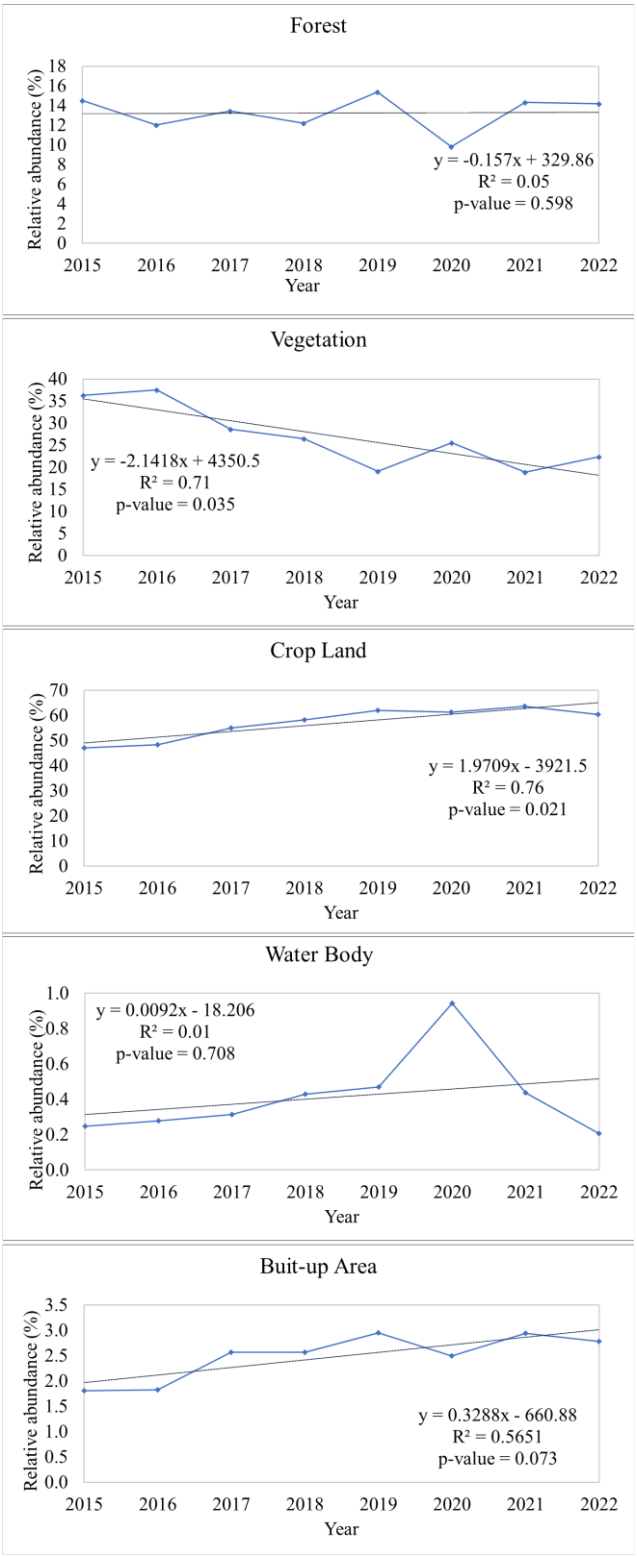

Fig. 7. Time Series of LULC from 2015 to 2022

An increase in built-up areas indicates ongoing urbanization and infrastructure development, contributing to the reduction in vegetation cover and the expansion of agricultural land and urbanization [24], and this correlation was also seen in this study The decrease in the forest cover exposes underlying litho-minerals such as iron oxide and clay, increasing their visibility and potentially leading to a decline in clay content due to the loss of organic matter affecting soil structure [25], [26]. The significant drop in vegetation reduces soil protection and affects clay minerals, essential for maintaining soil fertility. Cropland and water body ($r = 0.55$, $p < 0.01$) show that agricultural activities are often concentrated near water bodies, critical for irrigation and crop production, especially during dry seasons or low rainfall periods [25]. Cropland and built-up areas ($r = 0.85$, $p < 0.0001$) and water bodies with built-up areas ($r = 0.6$, $p < 0.001$) indicate that croplands are often found near or within expanding urban areas, where farming is conducted on the outskirts of cities to supply urban markets [30]. Alternatively, this might reflect the conversion of agricultural lands into urbanization as cities grow [31]. The increase in cropland involves significant soil disturbance, revealing and concentrating iron oxides, which improve soil conditions for agriculture [15]. While, the expansion of built-up areas involves considerable land conversion, exposing underlying minerals such as iron oxide and clay, and disrupting natural mineral deposit patterns [27], [28]. Water and built-up areas have a moderate correlation ($r = 0.6$, $p < 0.001$), driven by the need for water in agricultural activities and infrastructure development [32]. The slight increase in water body cover affects sediment transport and deposition patterns, influencing mineral distribution in adjacent catchment. Moreover, correlations between vegetation and other classes, such as cropland, water bodies, and built-up areas, have occurred on clay and iron oxide.

Table 1. Pearson's correlation between LULC classes

	Forest	Vegetation	Crop Land	Water Body	Built-up Area
Forest	1				
Vegetation	0.09	1			
Crop Land	-0.86****	-0.45	1		
Water Body	-0.67**	0.06	0.55**	1	
Built-up Area	-0.95****	-0.2	0.85****	0.6***	1

The stars denote the significance levels of the correlation between independent variables: ****p-value <0.0001, ***p-value <0.001, **p-value <0.01, and *p-value <0.05.

4. CONCLUSION

This study has demonstrated the changes in land use and land cover (LULC) distribution associated with litho-mineral alteration in the Chrey Bak catchment. The study reveals that land conversion (from forest to agriculture) and urbanization have increased exposure to mineral-rich zones, particularly those containing iron oxide and clay. The current study offers insights into the distribution of LULC classes and their relationships across the litho-mineral alteration, with implications for the sustainable management of land cover resources and the Tonle Sap ecosystems. It is crucial for sustainable land management and mineral resource planning.

ACKNOWLEDGMENTS

We gratefully acknowledge the support Khmer Earth Observation Laboratory (KHEOBS), the Institute of Technology of Cambodia (ITC), and the French National Research Institute for Sustainable Development (IRD).

REFERENCES

[1] J. L. Kouassi, A. Gyau, L. Diby, Y. Bene, and C. Kouamé, "Assessing land use and land cover change and farmers' perceptions of deforestation and land degradation in south-west Côte d'Ivoire,West Africa," *Land*, vol. 10, no. 4, 2021, doi: 10.3390/land10040429.

[2] R. Lal, "Soil degradation by erosion.Land degradation Dev.," *L. Degrad. Dev.*, vol. 539, no. 2001, pp. 519–539, 2001.

[3] J. A. Foley *et al.*, "Global consequences of land use," *Science (80-.).*, vol. 309, no. 5734, pp. 570–574, 2005, doi: 10.1126/science.1111772.

[4] R. L. Chazdon, "Beyond deforestation: Restoring forests and ecosystem services on degraded lands," *Science (80-.).*, vol. 320, no. 5882, pp. 1458–1460, 2008, doi: 10.1126/science.1155365.

[5] V. S. Bhagat, "Use of Remote Sensing Techniques for Robust Digital Change Detection of Land: A Review," *Recent Patents Sp. Technol.*, vol. 2, no. Cd, p. 123+144, 2012.

[6] A. Imbroane, C. Melenti, and D. Gorgan, "Mineral explorations by landsat image ratios," *Proc. - 9th Int. Symp. Symb. Numer. Algorithms Sci. Comput. SYNASC 2007*, no. September 2007, pp. 335–340, 2007, doi: 10.1109/SYNASC.2007.52.

[7] K. Zaw *et al.*, "Tectonics and metallogeny of mainland Southeast Asia - A review and contribution," *Gondwana Res.*, vol. 26, no. 1, pp. 5–30, 2014, doi: 10.1016/j.gr.2013.10.010.

[8] I. Yang and T. D. Acharya, "Exploring Landsat 8," *Int. J. IT, Eng. Appl. Sci. Res.*, vol. 4, no. 4, pp. 4–10, 2015, [Online]. Available: https://www.researchgate.net/profile/Tri-Acharya/publication/311901147_Exploring_Landsat_8/links/589c0de6458515e5f4549e58/Exploring-Landsat-8.pdf%0Ahttp://earthobservatory.nasa.gov/IOTD/

[9] M. Area, "Effect of Different Atmospheric Correction Algorithms on Sentinel-2 Imagery Classification Accuracy in a Semiarid Mediterranean Area," 2021.

[10] D. Phiri *et al.*, "remote sensing Sentinel-2 Data for Land Cover / Use Mapping : A Review," *Remote Sens.*, vol. 42, no. 3, p. 14, 2019.

[11] R. Manandhar, I. O. A. Odehi, and T. Ancevt, "Improving the accuracy of land use and land cover classification of landsat data using post-classification enhancement," *Remote Sens.*, vol. 1, no. 3, pp. 330–344, 2009, doi: 10.3390/rs1030330.

[12] C. Kamusoko, "Land Cover Classification Accuracy Assessment," *Springer Geogr.*, vol. 80, pp. 105–118, 2022, doi: 10.1007/978-981-16-5149-6_6.

[13] A. B. Pour and M. Hashim, "The application of ASTER remote sensing data to porphyry copper and epithermal gold deposits," *Ore Geol. Rev.*, vol. 44, pp. 1–9, 2012, doi: 10.1016/j.oregeorev.2011.09.009.

[14] A. Sheikhrahimi, A. B. Pour, B. Pradhan, and B. Zoheir,

"Mapping hydrothermal alteration zones and lineaments associated with orogenic gold mineralization using ASTER data: A case study from the Sanandaj-Sirjan Zone, Iran," *Adv. Sp. Res.*, vol. 63, no. 10, pp. 3315–3332, 2019, doi: 10.1016/j.asr.2019.01.035.

[15] A. Y. Yesuph and A. B. Dagnew, "Land use/cover spatiotemporal dynamics, driving forces and implications at the Beshillo catchment of the Blue Nile Basin, North Eastern Highlands of Ethiopia," *Environ. Syst. Res.*, vol. 8, no. 1, 2019, doi: 10.1186/s40068-019-0148-y.

[16] S. Gaur and R. Singh, "A Comprehensive Review on Land Use/Land Cover (LULC) Change Modeling for Urban Development: Current Status and Future Prospects," *Sustain.* , vol. 15, no. 2, 2023, doi: 10.3390/su15020903.

[17] Sociedad Canadiense del suelo, "Digging into Canadian Soils: An Introduction to Soil Science," pp. 62–68, 2024.

[18] M. Čengić *et al.*, "Global Maps of Agricultural Expansion Potential at a 300 m Resolution," *Land*, vol. 12, no. 3, 2023, doi: 10.3390/land12030579.

[19] Y. Wu, P. Qian, L. Yang, Z. Tian, and J. Luo, "Analysis of the Impact of Urban Infrastructure on Urbanization Processes at Different Levels from a Spatiotemporal Perspective," *Sustain.*, vol. 16, no. 16, 2024, doi: 10.3390/su16166888.

[20] B. Nyberg, R. Sayre, and E. Luijendijk, "Increasing seasonal variation in the extent of rivers and lakes from 1984 to 2022," *Hydrol. Earth Syst. Sci.*, vol. 28, no. 7, pp. 1653–1663, 2024, doi: 10.5194/hess-28-1653-2024.

[21] Y. Chen, Y. Wang, F. Zhang, Y. Dong, Z. Song, and G. Liu, "Remote Sensing for Lithology Mapping in Vegetation-Covered Regions: Methods, Challenges, and Opportunities," *Minerals*, vol. 13, no. 9, pp. 1–26, 2023, doi: 10.3390/min13091153.

[22] P. Potapov *et al.*, "The Global 2000-2020 Land Cover and Land Use Change Dataset Derived From the Landsat Archive: First Results," *Front. Remote Sens.*, vol. 3, no. April, pp. 1–22, 2022, doi: 10.3389/frsen.2022.856903.

[23] L. Yang, L. Shi, J. Li, and H. Kong, "Spatio-temporal pattern change of LULC and its response to climate in the Loess Plateau, China," *Sci. Rep.*, vol. 14, no. 1, p. 23202, 2024, doi: 10.1038/s41598-024-73945-0.

[24] P. Longobardi, A. Montenegro, H. Beltrami, and M. Eby, "Deforestation induced climate change: Effects of spatial scale," *PLoS One*, vol. 11, no. 4, 2016, doi: 10.1371/journal.pone.0153357.

[25] D. C. Rey-Romero, I. Domínguez, and E. R. Oviedo-Ocaña, "Effect of agricultural activities on surface water quality from páramo ecosystems," *Environ. Sci. Pollut. Res.*, vol. 29, no. 55, pp. 83169–83190, 2022, doi: 10.1007/s11356-022-21709-6.

[26] D. S. E. Bramble *et al.*, "Formation of mineral-associated organic matter in temperate soils is primarily controlled by mineral type and modified by land use and management intensity," *Glob. Chang. Biol.*, vol. 30, no. 1, pp. 1–19, 2024, doi: 10.1111/gcb.17024.

[27] K. A. Locke, "Impacts of land use/land cover on water quality: A contemporary review for researchers and policymakers," *Water Qual. Res. J.*, vol. 59, no. 2, pp. 89–106, 2024, doi: 10.2166/wqrj.2024.002.

[28] M. L. T. Santana *et al.*, "Impacts of Land Use Changes on Soil Functions and Water Security: Insights from a Three-Year-Long Study in the Cantareira System, Southeast of Brazil," *Sustain.*, vol. 15, no. 18, 2023, doi: 10.3390/su151813395.

[29] R. Kong *et al.*, "Understanding the drivers of deforestation and agricultural transformations in the Northwestern uplands of Cambodia," *Appl. Geogr.*, vol. 102, no. November 2018, pp. 84–98, 2019, doi: 10.1016/j.apgeog.2018.12.006.

[30] H. Ju *et al.*, "The changing patterns of cropland conversion to built-up land in China from 1987 to 2010," *J. Geogr. Sci.*, vol. 28, no. 11, pp. 1595–1610, 2018, doi: 10.1007/s11442-018-1531-8.

[31] Y. Yan, X. Liu, and Y. Wen, "Quantification of the Relationship Among Cropland Area, Cropland Management Measures, and Cropland Productivity Using Panel Data Model," *Int. J. Plant Prod.*, vol. 14, no. 4, pp. 689–702, 2020, doi: 10.1007/s42106-020-00113-5.

[32] F. Wang and C. Gao, "Settlement–river relationship and locality of river-related built environment," *Indoor Built Environ.*, vol. 29, no. 10, pp. 1331–1335, 2020, doi: 10.1177/1420326X20976500.